GT2018-76921

DRAFT: THERMOACOUSTIC MODES OF QUASI-1D COMBUSTORS IN THE REGION OF MARGINAL STABILITY

Camilo F. Silva***, Kah Joon Yong**

Professur für Thermofluiddynamik
Technische Universität München
Email: silva@tfd.mw.tum.de

Luca Magri

University of Cambridge
Engineering Department
Cambridge, UK

ABSTRACT

It may be generally believed that the thermoacoustic eigenfrequencies of a combustor with fully acoustic reflecting boundary conditions depend on both flame dynamics and geometry of the system. In this work, we show that there are situations where this understanding does not strictly apply.

The purpose of this study is twofold. In the first part, we show that the resonance frequencies of two premixed combustors with fully acoustic reflecting boundary conditions in the region of marginal stability depend only on the parameters of the flame dynamics, but do not depend on the combustor's geometry. This is shown by means of a parametric study, where the time delay and the interaction index of the flame response are varied and the resulting complex eigenfrequency locus is shown. Assuming longitudinal acoustics and a low Mach number, a quasi-1D Helmholtz solver is utilized. The time delay and interaction index of the flame response are parametrically varied to calculate the complex eigenfrequency locus. It is found that all locus trajectories cross the real axis at a resonance frequency that depends only on the time delay and is independent of the resonant cavity modes, i.e. the passive thermoacoustic modes, of the two combustors.

In the second part, we exploit the aforementioned observation to evaluate the critical flame gain required for the systems to become unstable at four eigenfrequencies located in the marginally stable region. A computationally-efficient method is proposed. The key ingredient is to consider both direct and

adjoint eigenvectors associated with the four eigenfrequencies. Hence, the sensitivity of the gain to changes in the eigenfrequencies at the region of marginal stability is evaluated with cheap and accurate calculations.

By presenting a methodology to compute critical gains of the flame response and corresponding sensitivity, this work aims to contribute to the conception of thermoacoustic stable combustors. In the same manner, the understanding of the origin of distinct resonance frequencies in unstable combustors may be enhanced by employing the analysis of the eigenfrequency locus here reported.

INTRODUCTION

Thermoacoustic instabilities in combustion chambers of gas turbines and rockets are persistent and intractable problems that industry faces. Such instabilities are due to the two-way coupling between the unsteady heat release rate produced during combustion and the acoustic waves originated by the volumetric expansion in the reactive region [1, 2]. If a thermoacoustic instability is triggered, very large amplitude of pressure fluctuations arise, which may lead to critical failures of the system. One well-known technique for the study of thermoacoustic instabilities is based on a divide-and-conquer approach. On the one hand, the flame response to incoming acoustic perturbations is evaluated either experimentally or numerically [3–6]. On the other hand, the system acoustics is investigated by means of partial differential equations, such as the Helmholtz equation or the

---

linearized Navier-Stokes equations, or through acoustic network models [7–10]. Finally, an eigenvalue problem is defined, where the flame response is introduced in the equations characterizing the acoustics of the system. The solution of the eigenvalue problem provides the resonance frequency and growth rate of the thermoacoustic modes of interest. Attention is generally given to thermoacoustic modes evaluated to be unstable, where the growth rate is positive, or marginally stable, where the growth rate is close to zero.

Thermoacoustic systems with fully or partially acoustic reflecting boundary conditions that do no contain any flame dynamics (the gain of the flame response being zero) are characterized by *passive* thermoacoustic modes[1]. For example, the acoustics of a duct system described with Neumann (closed inlet) and Dirichlet (open outlet) boundary conditions at low frequency is characterized by a quarter-wave thermoacoustic mode. It has been generally understood that once the dynamics of the flame is taken into account, this mode may be enhanced or suppressed by its interaction with the heat release rate emitted by the flame. Let us discuss a brief example. When the flame response is described by a $n - \tau$ model [11, 12], such a system can be considered stable in situations when the time delay τ is smaller than half of the thermoacoustic period [13]. Thus, considering both the flame dynamics, here described by the $n - \tau$ model, and the system's acoustics, here characterized by the period of the quarter-wave thermoacoustic mode, is essential for the assessment of the thermoacoustic stability of the system.

Over the last few years, the understanding of thermoacoustics has been extended by the discovery of Intrinsic ThermoAcoustic (ITA) instabilities [6, 14–16]. It was found that systems with anechoic boundary conditions, and therefore deprived of any type of passive acoustic modes directly linked to the system's geometry, can also exhibit thermoacoustic instabilities. The ITA feedback loop can be briefly explained as follows. Velocity perturbations upstream of the flame induce fluctuations of heat release rate, which in turn generate acoustic fluctuations. Subsequently, the upstream acoustic travelling waves influence the velocity disturbances upstream of the flame, thereby closing the ITA loop. Based on a $n - \tau$ flame response model, a stability criterion was obtained for anechoic systems by Hoeijmakers et al. [14] and Emmert et al. [15]. It was found that Intrinsic ThermoAcoustic (ITA) modes, which are characterized by a resonance frequency $f = j/(2\tau)$ (where $j = 1, 3, 5, \cdots$ is an odd number) are unstable if the interaction index is larger than a critical value that is function mainly of the temperature ratio. By investigating a turbulent swirled combustor with partially reflecting boundary conditions and a frequency-dependent flame response, Silva et al. [17] subsequently found that the ITA feedback loop plays an important role not only in the stability of the system but

also in the generation of combustion noise.

Moreover, when considering systems with fully reflecting conditions, it was found by Mukherjee and Shrira [18] that the ITA resonance frequencies at the neutral curve (when the growth rate is exactly zero) is the same as the one associated with the ITA modes in anechoic systems $f = j/(2\tau)$. Therefore, it was concluded that the resonance frequency at the neutral curve of the ITA modes in systems with fully reflecting acoustic boundary conditions is *independent* of the system's geometry.

Based on the study of thermoacoustic systems with fully acoustic reflecting boundary conditions, the present work aims to show that, aside from passive thermoacoustic modes, *all* resonance frequencies at the neutral curve within the frequency band considered depend exclusively on the flame dynamics and dot not depends on the geometry of the combustor. These modes, recognized here as ITA modes because of their exclusive dependence on the flame dynamics, are the *only* (active) thermoacoustic modes present at the neutral curve. Importantly, the stability of ITA modes is strongly related to a critical gain. In this work, a computationally-efficient methodology is proposed to exactly calculate the critical gain of a given ITA thermoacoustic mode. Beyond such a critical gain, instability is predicted to occur. By analyzing the structure of both direct and adjoint thermoacoustic modes at the marginally stable region, we explain why some configurations exhibit critical gains that are much larger (or smaller) than other configurations. The methodology proposed is applied to combustors with three-coaxial ducts and a compact flame. It can be applied to any type of combustor's geometry when a stability solver is available to build the eigenvalue problem.

The paper is organized as follows. In the next section the quasi-1D Helmholtz equation is derived. Subsequently, two premixed combustors are investigated. A locus of the eigenfrequencies, which results from performing systematic variations of two parameters of the flame response, is computed by solving the nonlinear eigenvalue problem corresponding to the Helmholtz equation. Afterwards, a method is proposed to compute in an efficient way the direct and adjoint eigenvectors, in addition to the critical gain and corresponding sensitivity at the neutral curve. Finally, the obtained results are presented and the thermoacoustic stability of the two combustors investigated is analyzed.

THE QUASI-1D HELMHOLTZ EQUATION

Since we are interested in thermoacoustic systems that exhibit frequencies smaller than the cut-on frequency of transversal modes, we focus on quasi-1D systems, i.e systems where only longitudinal acoustic modes are modeled. Additionally, if a low Mach number flow is considered, the momentum and energy

---

[1]Note that the mean fields of temperature and density are still affected by the flame.

conservation equations read, respectively

$$\bar{\rho}\frac{\partial u'}{\partial t} + \frac{\partial p'}{\partial x} = 0 \qquad (1)$$

$$\frac{S}{\bar{\rho}\bar{c}^2}\frac{\partial p'}{\partial t} + \frac{\partial}{\partial x}\left(Su'\right) = \frac{(\gamma-1)}{\bar{\rho}\bar{c}^2}\dot{q}'S, \qquad (2)$$

where u, p and $\dot{q}$ denote velocity, pressure and heat release rate. The quantities ρ, c, γ and S stand for density, speed of sound, heat capacity ratio and cross-section area, respectively. The symbols $\bar{[\ ]}$ and $[\ ]'$ represent mean and fluctuating quantities. Subtracting the spatial derivative of Eqn. (1) to the temporal derivative of Eqn. (2) results in

$$\frac{1}{S}\frac{\partial}{\partial x}\left(S\bar{c}^2\frac{\partial \hat{p}}{\partial x}\right) + \omega^2\hat{p} = -i\omega(\gamma-1)\hat{q}, \qquad (3)$$

where the harmonic transformation $[\ ]' = \hat{[\ ]}e^{i\omega t}$ has been applied. By assuming that the flame is acoustically compact, i.e. the flame length is negligible with respect to the acoustic wavelength, the local heat release rate $\hat{q}$ can be expressed in terms of the global heat release rate $\hat{Q}$ as $\hat{q} = I_d\hat{Q}/V_f$, where V_f is the volume of the flame [9]. The vector I_d is equal to one for nodes inside the flame and zero elsewhere. We express now $\hat{Q} = \hat{Q}_c + \hat{Q}_n$, where $\hat{Q}_c$ represents the heat release rate coupled with upstream velocity perturbations and $\hat{Q}_n$ denotes the heat release rate correlated to random turbulence fluctuations. By considering that $V_f = S_f\, l_f$, where l_f is a characteristic flame length, Eqn. (3) becomes

$$\frac{1}{S}\frac{\partial}{\partial x}\left(S\bar{c}^2\frac{\partial \hat{p}}{\partial x}\right) + \omega^2\hat{p} + i\omega(\gamma-1)I_d\hat{Q}_c/(S_f\, l_f)$$
$$= -i\omega(\gamma-1)I_d\hat{Q}_n/(S_f\, l_f). \qquad (4)$$

The heat release rate associated to $\hat{Q}_c$ can be related to upstream velocity perturbations at a reference position $\hat{u}_{ref}$ by means of the flame transfer function $\mathscr{F}(\omega)$, defined as as

$$\frac{\hat{Q}_c}{\bar{\dot{Q}}} = \mathscr{F}(\omega)\frac{\hat{u}_{ref}}{\bar{u}_{ref}}. \qquad (5)$$

We express now the mean heat release rate as $\bar{\dot{Q}} = \bar{\rho}_{ref}\bar{u}_{ref}S_{ref}c_p T_u\theta$, where c_p is the specific heat capacity at constant pressure and $\theta = T_d/T_u - 1$ is the relative temperature increment across the flame. The indices 'u' and 'd' denote 'upstream' and 'downstream' of the flame, respectively. Thus, the quantity

$i\omega(\gamma-1)\hat{Q}_c$ can be expressed as

$$i\omega(\gamma-1)\hat{Q}_c = i\omega\bar{\rho}_{ref}\bar{c}_{ref}^2 S_{ref}\theta\mathscr{F}(\omega)\hat{u}_{ref} = -\bar{c}_{ref}^2 S_{ref}\theta\mathscr{F}(\omega)\left.\frac{\partial \hat{p}}{\partial x}\right|_{ref},$$
$$(6)$$

where the momentum equation (1), re-written as $\hat{u} = \frac{-1}{i\omega\bar{\rho}}\frac{\partial\hat{p}}{\partial x}$, has been considered. Finally, the Helmholtz equation for quasi-1D acoustic systems reads

$$\underbrace{\frac{1}{S}\frac{\partial}{\partial x}\left(S\bar{c}^2\frac{\partial\hat{p}}{\partial x}\right)}_{\mathscr{A}\,\hat{p}} - \underbrace{K\mathscr{F}(\omega)\left.\frac{\partial\hat{p}}{\partial x}\right|_{ref}}_{\mathscr{H}\mathscr{F}(\omega)\hat{p}} + \underbrace{\omega^2\hat{p}}_{-\sigma\hat{p}} = -i\omega(\gamma-1)\hat{Q}_n/(S_f\, l_f)$$
$$(7)$$

where $K = I_d\alpha\theta\bar{c}_{ref}^2/l_f$ and $\alpha = S_{ref}/S_f$. In the present study, we are interested in the Helmholtz equation and the corresponding eigenvalue problem. After dropping the forcing term from the formulation, the eigenvalue problem obtained reads:

$$\left(\mathscr{A} - \mathscr{H}\mathscr{F}(\omega_k)\right)\hat{p}_k = \sigma_k\hat{p}_k \quad \Rightarrow \quad \mathscr{L}\hat{p}_k = \sigma_k\hat{p}_k \qquad (8)$$

where $\hat{p}_k$ denotes the k_{th} acoustic mode and ω_k the corresponding complex eigenfrequency, which in turn is linked to the k_{th} eigenvalue by $\sigma_k = -\omega_k^2$. In the present work, the nonlinear eigenvalue problem given by Eqn. (8) is solved by means of an in-house Helmholtz solver based on a finite-difference numerical scheme. A methodology based on a fixed-point iteration with relaxation, which is similar to that of Silva et al. [9], was implemented.

THE LOCUS OF THE EIGENFREQUENCIES AROUND THE FIRST LONGITUDINAL ACOUSTIC MODE

One of the objectives of this work is to understand the structure of both ITA and classical thermoacoustic modes at the marginal region of stability. Before performing such an analysis, we plot the locus of the eigenfrequencies given by Eqn. (8) around the first passive thermacoustic mode. The analysis being carried out in this section can be performed around any other passive thermoacoustic mode.

Two premixed combustors

Two different configurations are studied. The first configuration, here denoted 'Duct', is a duct flame previously studied in the work of Hoeijmakers et al. [14]. The second configuration, here denoted 'BRS', is a premixed swirled combustor previously studied in the works of [5, 17, 19, 20]. Figure 1 illustrates these two configurations, and Tab. 1 shows the geometrical and thermodynamic parameters of interest. In this study, the inlet boundary condition is defined as Neumann $\partial\hat{p}/\partial x = 0$, whereas the
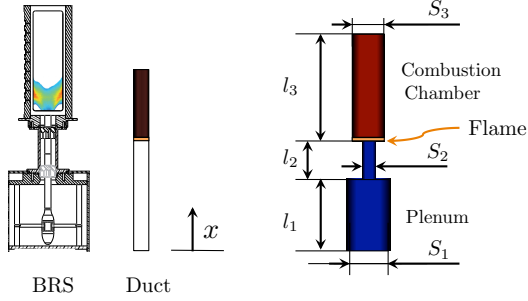
outlet is defined as Dirichlet $\hat{p} = 0$.

FIGURE 1. The two configurations under investigation. Corresponding dimensions and thermodynamics parameters are given in Tab. 1.

TABLE 1. Geometrical and thermodynamic parameters of the two configurations under investigation.

Parameter	BRS	Duct
l_1 (m)	0.17	0.15
l_2 (m)	0.18	0.15
l_3 (m)	0.336	0.2
S_1 (m^2)	$\pi/4 \, 0.2^2$	1
S_2 (m^2)	$\pi/4 \, (0.04^2 - 0.016^2)$	1
S_3 (m^2)	0.09^2	1
$\bar{T}_u$ (K)	293	293
$\bar{T}_d$ (K)	1930	1600
$\bar{\rho}_u$ (kg/m^3)	1.204	1.204
$\bar{\rho}_d$ (kg/m^3)	0.183	0.22
$\bar{c}_u$ (m/s)	343	343
$\bar{c}_d$ (m/s)	881	774

The first passive thermoacoustic mode $\hat{p}_{1p}$, shown in Fig. 2, and corresponding eigenfrequency ω_{1p} are obtained by solving Eqn. (8) with $\mathcal{F}(\omega) = 0$. On the one hand, the first thermoacoustic mode of the 'Duct' configuration is associated with the quarter-wave mode of the duct with $\omega_{1p} = 2\pi \cdot 250$ rad/s. On the other hand, the first thermoacoustic mode of the 'BRS' configuration is the Helmholtz mode of the plenum with $\omega_{1p} = 2\pi \cdot 55$ rad/s.
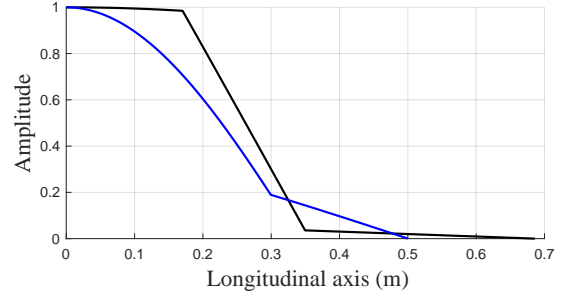

FIGURE 2. First passive thermoacoustic mode $\hat{p}_{1p}$. (Blue) Duct, (Black) BRS.

The loci of eigenfrequencies

In this study, the flame response is described by an $n - \tau$ model so that $\mathcal{F}(\omega) = ne^{-i\omega\tau}$, where n is the interaction index and τ denotes a characteristic time delay. We carry out a parametric study by varying $n = [0 \rightarrow 1]$ for the Duct configuration and $n = [0 \rightarrow 4]$ for the BRS configuration. The time delay is varied as $\tau = [0 \rightarrow 2\pi/\omega_{1p}]$ for both configurations. The corresponding eigenfrequencies, which are solutions of Eqn. (8), are plotted in the complex plane. Figures 3 and 4 show the results for the Duct configuration and 'BRS' combustor, respectively.

Although the two configurations are different, the loci obtained have strong similarities. In both Duct and BRS cases we observe a star-like structure and curvilinear trajectories. The center of the star is given by the eigenfrequency of the passive acoustic mode ω_{1p}. Once n is increased from zero, the eigenfrequencies depart from ω_{1p}. These trajectories rotate counter clock-wise for increments of τ. We can observe that some trajectories reach instability (growth rate > 0) for $n > n_{g_0}$, where n_{g_0} denotes a critical value for the interaction index.

Let us now concentrate on the trajectories connected to the star center ω_{1p} and defined by $\tau = m \cdot 2\pi/\omega_{1p}$ with $0.32 < m < 0.33$ (dashed lines in Figs. 3 and 4). We observe that these trajectories change direction suddenly (from left to right when increasing m) after a critical value $m_c \approx 0.325$, which corresponds to $\tau_c \approx 1.3$ ms for the Duct configuration and $\tau_c \approx 5.9$ ms for the BRS combustors. This behavior can be considered as a bifurcation: given $n > n_{g_0}$ a slight increment in τ from $\tau < \tau_c$ to $\tau > \tau_c$ can transform a robust stable combustor to a highly unstable one.

From Figs. 3 and 4 it is also possible to observe quasi-vertical trajectories whose growth rate for small values of n is very negative and increases for increments of n. As observed also by Mukherjee and Shrira [18], the resonance frequency tends to real$(\omega) = 2\pi \cdot j/(2\tau)$ (with $j = 1, 3, 5, \cdots$) and Imag$(\omega) = -\infty$ when n approaches zero, as illustrated in Fig. (5) for the duct configuration. The real part of this frequency corresponds to ITA resonance frequencies [14, 15]. Correspondingly, we label these trajectories as ITA trajectories[2]. A crucial observation results by looking at the resonance frequencies for *zero* growth rates. As
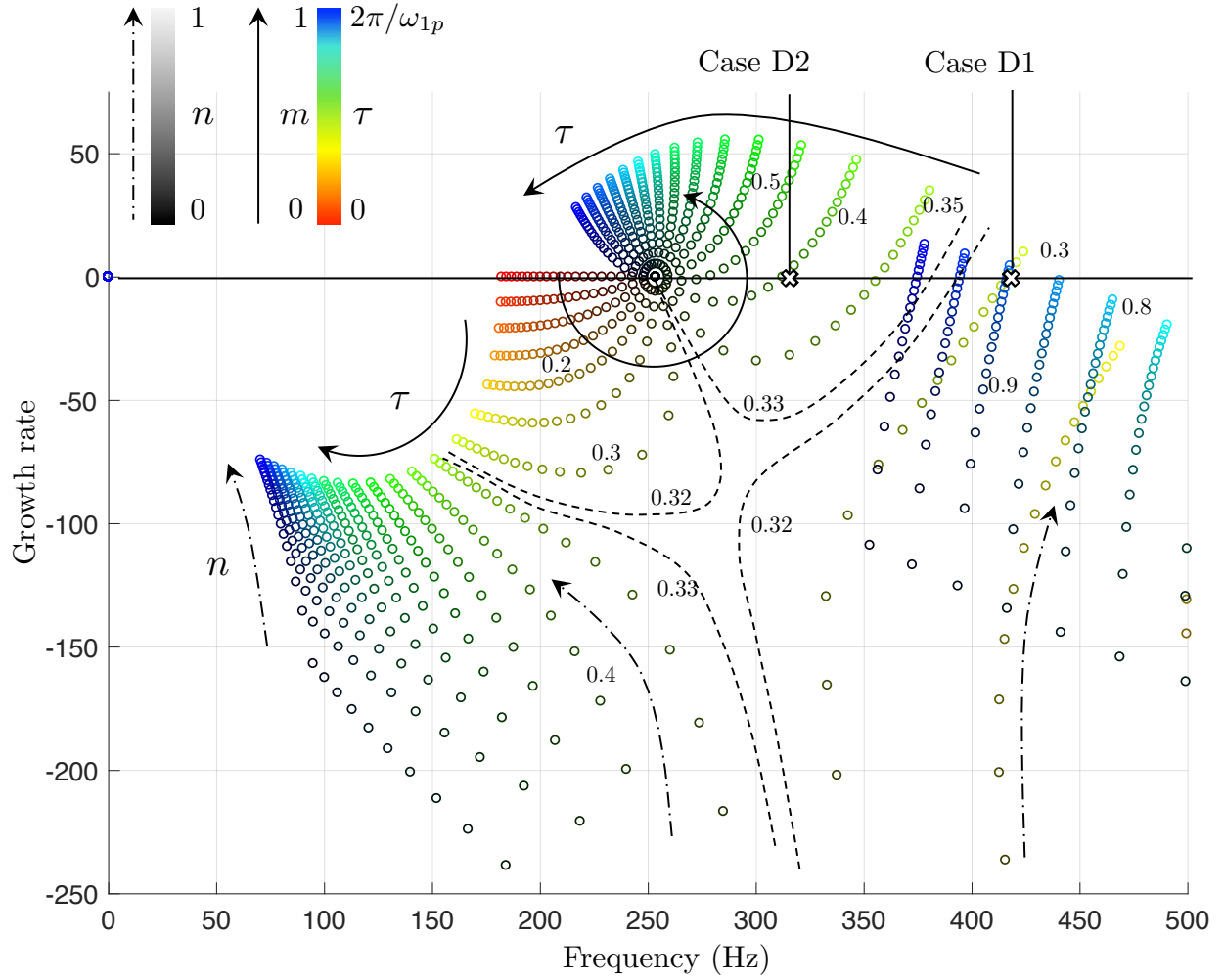
FIGURE 3. Locus of eigenfrequencies on the complex plane that corresponds to the Duct configuration. $n = [0 \rightarrow 1]$ with $\Delta n = 0.05$ and $\tau = [0 \rightarrow 2\pi/\omega_{1p}]$. $\tau = m \cdot 2\pi/\omega_{1p}$ with $m = 0 \rightarrow 1$ and $\Delta m = 0.05$. Numbers in the plot are values of m for the closest trajectory. The growth rate is defined as $-\text{Im}(\omega)/2\pi$.

already pointed out by Mukherjee and Shrira [18], this value is equal to $\text{real}(\omega) = 2\pi \cdot j/(2\tau)$ for the ITA trajectories. In addition, from Figs. 3 and 4 it is observed that this is also the case for the trajectories that belong to the star-like structure and cross the real axis (for $m = 0.35, 0.4, 0.45$). Indeed, it is observed in an extended plot (Fig. 5) that the resonance frequency at zero growth rate corresponding to *all* trajectories that cross the real-axis over the investigated range of $0 < \text{real}(\omega) < 2\pi \cdot 1000$ is function exclusively of the time delay τ. This finding is of interest for stability analysis of thermoacoustic systems since it establishes potential resonance frequencies in unstable combustors. As shown in the next section, this funding also allows us to efficiently com-

pute the eigentriplet $\hat{p}_k$, $\hat{p}_k^\dagger$, ω_k at the neutral curve.

THE INTERACTION INDEX AT THE MARGINAL REGION OF STABILITY

So far we have observed in Figs. 3 and 4 that all trajectories crossing the real axis exhibit a resonance frequency $\text{real}(\omega) = 2\pi \cdot j/(2\tau)$ (with $j = 1, 3, 5, \cdots$) at zero growth rate. The purpose of this section is to show a computationally efficient technique that exploits this observation in order to compute the value

---

[2]Solving the nonlinear eigenvalue problem (Eqn. (8)) to find ITA trajectories is numerically more challenging. It was necessary to apply small relaxation factors (around 0.005) to the fix-point algorithm used to reach convergence.
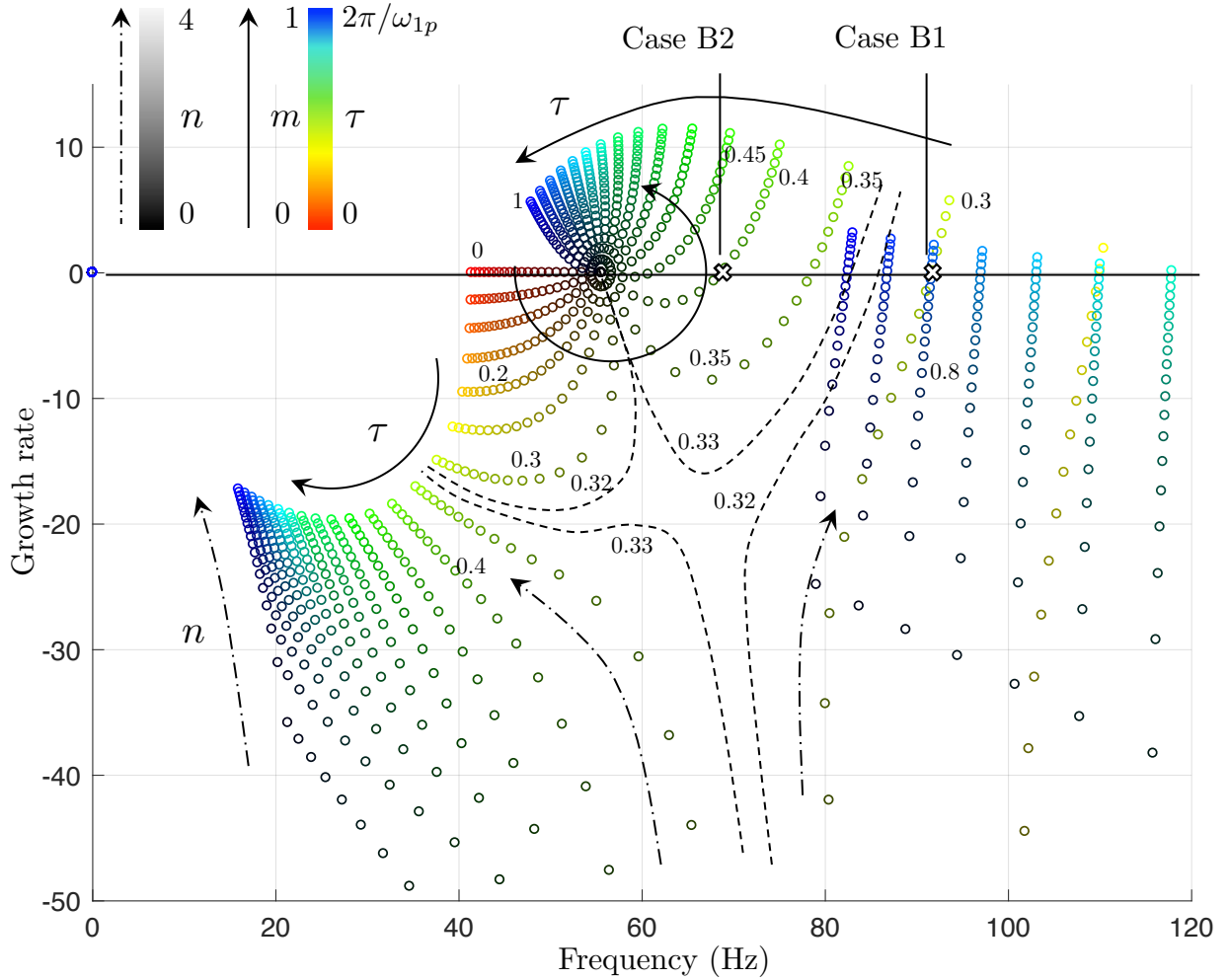
FIGURE 4. Locus of eigenfrequencies in the complex plane of the BRS configuration. $n = [0 \rightarrow 4]$ with $\Delta n = 0.2$ and $\tau = [0 \rightarrow 2\pi/\omega_{1p}]$. $\tau = m \cdot 2\pi/\omega_{1p}$ with $m = 0 \rightarrow 1$ and $\Delta m = 0.05$. Numbers in the plot are values of m for the closest trajectory. The growth rate is defined as $-\text{Im}(\omega)/2\pi$.

of the interaction index n_{g_0}, which corresponds to the eigenfrequency $\omega_{g_0} = 2\pi \cdot j/(2\tau) + i \cdot 0$. Subsequently, the sensitivity $\partial \omega/\partial n|_{\omega=\omega_{g_0}}$ is evaluated by with a computationally-efficient and accurate adjoint approach [21, 22].

The direct and adjoint eigenvectors

The adjoint eigenvalue problem reads

$$\mathscr{L}^\dagger \hat{p}_k^\dagger = \sigma_k^\dagger \hat{p}_k^\dagger, \tag{9}$$

where the symbol $[\ ]^\dagger$ denotes 'adjoint'. The adjoint eigenvalue $\sigma^\dagger$ is equal to the complex conjugate of σ, i.e. $\sigma^\dagger = \sigma^*$ and the adjoint operator $\mathscr{L}^\dagger$ is the conjugate transpose of $\mathscr{L}$, i.e.

$\mathscr{L}^\dagger = \mathscr{L}^H$ [23]. Furthermore, for the biorthogonality condition, $\langle \hat{p}_k^\dagger, \hat{p}_l \rangle = (\hat{p}_k^\dagger)^H \hat{p}_l$, is equal to zero for $k \neq l$. If in addition the direct and adjoint eigenvectors are normalized, we know that $\langle \hat{p}_k^\dagger, \hat{p}_k \rangle = (\hat{p}_k^\dagger)^H \hat{p}_k = 1$. Let us now project the direct eigenvalue problem (Eqn. (8)) for a given thermoacoustic mode $\hat{p}_k$ on the adjoint eigenvector $p_k^\dagger$. The new problem reads:

$$(\hat{p}_k^\dagger)^H \mathscr{L} \hat{p}_k = (\hat{p}_k^\dagger)^H \left(\mathscr{A} - \mathscr{H} n\, e^{-i\omega_k \tau} \right) \hat{p}_k = \sigma_k (\hat{p}_k^\dagger)^H \hat{p}_k = \sigma_k, \tag{10}$$
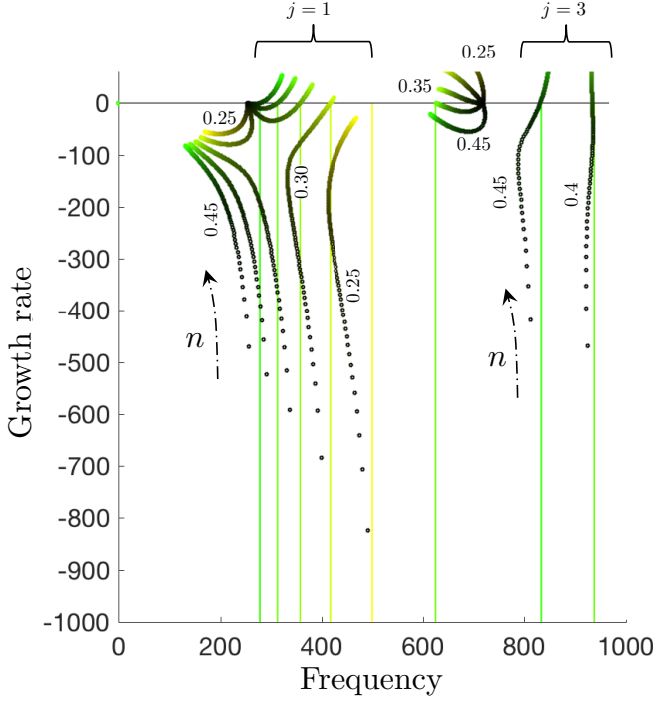
FIGURE 5. Locus of eigenfrequencies in the complex plane of the Duct configuration. $n = [0.005 \rightarrow 1]$ with $\Delta n = 0.005$. Numbers in the plot are values of m for the closest trajectory. Note that only the trajectories defined by $\tau = m \cdot 2\pi/\omega_{1p}$ with $m = 0.25 \rightarrow 0.45$ ($\Delta m = 0.05$) have been considered to preserve readability. Vertical lines indicate frequencies equal to $j/2\tau$.

Finally, Eqn. (10) is reorganized in terms of the interaction index n:

$$n = \frac{(\hat{p}_k^\dagger)^H \mathscr{A} \ \hat{p}_k + \omega_k^2}{(\hat{p}_k^\dagger)^H \mathscr{H} \ \hat{p}_k \ e^{-i\omega_k \tau}}. \qquad (11)$$

The calculation of the critical flame gain

Equation (11) tells us that a given value of n is directly related to the eigentriplet $\hat{p}_k$, $\hat{p}_k^\dagger$, ω_k and time delay τ, in addition to the acoustic and flame operators $\mathscr{A}$ and $\mathscr{H}$. In this study we calculate the value of n such that the eigenfrequency is marginal, i.e. it is equal to $\omega_{g_0} = 2\pi \cdot j/(2\tau) + i \cdot 0$. This critical value is denoted n_{g_0}. Therefore, in addition to $\mathscr{A}$ and $\mathscr{H}$, we know the quantities $\omega_k = \omega_{g_0}$ and τ. In contrast, the eigenvectors $\hat{p}_k$ and $\hat{p}_k^\dagger$ at the neutral curve still have to be evaluated. In principle, we must know n in order to solve the direct and adjoint eigenvalue problems given by Eqns. (8) and (9), respectively. We circumvent that difficulty as follows.

Let us refer now to the active thermoacoustic system given

by Eqn. (8), written now as

$$\mathscr{A}\hat{p}_k - \sigma_k\hat{p}_k = \underbrace{\mathscr{H}\mathscr{F}(\omega)\hat{p}_k}_{s_a} \qquad (12)$$

where s_a is a vector acting as a forcing term at the region of the flame. Since we don't know the value of the vector s_a, we choose a vector s with uniform forcing (and trivial value) at the region of the flame. In this study we make $s = I_d$, i.e. a vector equal to one at the region of the flame and zero elsewhere. Consequently, the vector s is proportional to s_a. The solution of Eqn. (12) with forcing term s is denoted $\tilde{p}_k$, and is considered proportional to $\hat{p}_k$ as explained in more detail in Appendix A. By carrying out a similar analysis we obtain $\tilde{p}_k^\dagger$, which is also assumed proportional to $\hat{p}_k^\dagger$. Finally, the estimated direct $\hat{p}_k$ and adjoint eigenvectors $\hat{p}_k^\dagger$ are obtained by normalizing $\tilde{p}_k$ and $\tilde{p}_k^\dagger$, so that $(\hat{p}_k^\dagger)^H\hat{p}_k = 1$ as explained in Appendix A.

Sensitivity study

In addition to estimating n_{g_0} from Eqn. (11), we evaluate $\partial\omega/\partial n|_{\omega_{g_0}}$, which is the sensitivity of ω with respect to small changes of n around the critical flame gain, n_{g_0}. By applying the chain rule, we obtain

$$\left.\frac{\partial\omega}{\partial n}\right|_{\omega_{g_0}} = \left(\frac{\partial\omega}{\partial\sigma}\frac{\partial\sigma}{\partial n}\right)_{\omega_{g_0}} \quad \text{where} \quad \frac{\partial\omega}{\partial\sigma} = \frac{-1}{2\omega}. \qquad (13)$$

Following [21, 22] and Silva et al. [24], we estimate $\partial\sigma/\partial n$ by means of a first-order adjoint formulation, which reads

$$\frac{\partial\sigma}{\partial n} = \frac{(\hat{p}_k^\dagger)^H \frac{\partial(\mathscr{L}-I\sigma)}{\partial n} \hat{p}_k}{(\hat{p}_k^\dagger)^H \frac{\partial(\mathscr{L}-I\sigma)}{\partial\sigma} \hat{p}_k} = \frac{(\hat{p}_k^\dagger)^H \mathscr{H}\hat{p}_k e^{-i\omega\tau}}{(\hat{p}_k^\dagger)^H \mathscr{H}\hat{p}_k \frac{i\,n\tau}{2\omega} e^{-i\omega\tau} + 1} \qquad (14)$$

Results

Let us concentrate on two eigenfrequencies with zero growth rate defined as $\omega_{g_0} = 2\pi \cdot 1/(2\tau) + i \cdot 0$ where $\tau = m \cdot 2\pi/\omega_{1p}$. The corresponding cases are denoted by D1($m = 0.3$) and D2 ($m = 0.4$) for the Duct configuration and B1 ($m = 0.3$) and B2 ($m = 0.4$) for the BRS combustor. These eigenfrequencies, displayed with a cross in Figs. 3 and 4, are arbitrarily chosen from the locus plot. It should be mentioned, however, that the case B1 lays on a locus of eigenfrequencies which are related to an ITA instability observed in the BRS combustor [17, 20]. Following the procedure described in the previous section, we solve the

7

linear systems

$$\mathscr{A}\tilde{\hat{p}}_k - \sigma_k \tilde{\hat{p}}_k = I_{\mathrm{d}} \quad \text{and} \quad \mathscr{A}^H \tilde{\hat{p}}_k^\dagger - \sigma_k^* \tilde{\hat{p}}_k^\dagger = I_{\mathrm{d}} \qquad (15)$$

where $\sigma_k = \sigma_k^* = -\omega_{g_0}^2$. Subsequently, the solutions $\tilde{\hat{p}}_k$ and $\tilde{\hat{p}}_k^\dagger$ are normalized by means of Eqn. (26) to obtain a first estimation of $\hat{p}$ and $\hat{p}^\dagger$. Results are shown in gray in Figs. (6) and (7) (although only distinguishable for $\hat{p}_k^\dagger$ in the region downstream of the flame). Next, we solve Eqn. (11) to obtain a first estimation of n_{g_0}. In order to obtain a better approximation of $\hat{p}$ and $\hat{p}^\dagger$, we solve

$$\mathscr{L}\tilde{\hat{p}}_k - \sigma_k \tilde{\hat{p}}_k = I_{\mathrm{d}} \quad \text{and} \quad \mathscr{L}^H \tilde{\hat{p}}_k^\dagger - \sigma_k^* \tilde{\hat{p}}_k^\dagger = I_{\mathrm{d}} \qquad (16)$$

where $\sigma_k = \sigma_k^* = -\omega_{g_0}^2$ and the values of n_{g_0} obtained previously are considered. Results are shown in Figs. (6) and (7) (in black although indistinguishable). These new evaluated eigenvectors $\hat{p}_k$ and $\hat{p}_k^\dagger$ are used to solve again Eqn. (11) to revaluate n_{g_0}. Tab. 2 shows the obtained values of n_{g_0} for the first and second iterations. In order to validate the estimated interaction index n_{g_0} and the corresponding eigenvectors $\hat{p}_k$ and $\hat{p}_k^\dagger$, we solve the nonlinear eigenvalue problem given by Eqn. (9) accounting for the estimated value n_{g_0} in the second iteration. Results are displayed in Figs. (6) and (7) (dashed blue and red lines). It is interesting to observe that the acoustic field related to $\hat{p}_k$ is very well estimated from the first iteration, and therefore gray, black and blue lines are exactly superposed. In addition, we see that the value of the eigenfrequency ω_k obtained by solving Eqn. (8) with the evaluated n_{g_0} is also very close to the one given by ω_{g_0}, as shown in Tab. 3. This verifies the proposed algorithm.

TABLE 2. Values of n_{g_0} obtained in first and second iterations for the four cases under investigation.

Parameter	Iteration	D1	D2	B1	B2
n_{g_0}	1	0.718	0.346	3.147	1.703
n_{g_0}	2	0.723	0.353	3.156	1.718

At the region of marginal stability, it is important not only to know the critical values for the interaction index n_{g_0}, but also to calculate the sensitivity of the eigenfrequency for a small change in n. Therefore, we apply Eqns. (13) and (14) to calculate $\partial\omega/\partial n|_{\omega_{g_0}}$ using the eigenvectors $\hat{p}_k$ and $\hat{p}_k^\dagger$ obtained in the second iteration of the method proposed. The sensitivity calculated with the adjoint method exactly matches the slope of the curve (Figs. 8 and 9). In other words, it is first-order accurate.
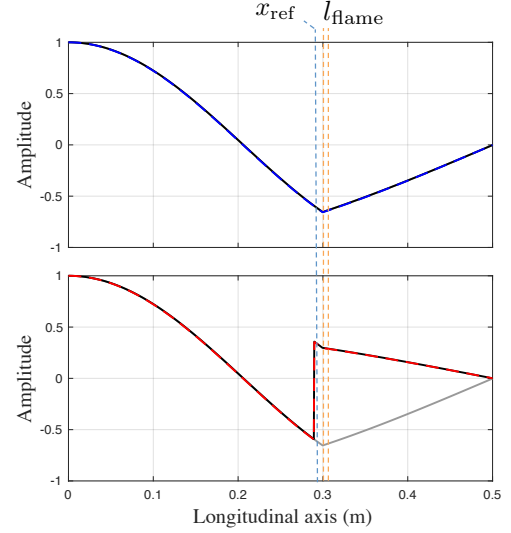

FIGURE 6. Thermoacoustic modes $\hat{p}/\max(\hat{p})$ (top) and $\hat{p}^\dagger/\max(\hat{p}^\dagger)$ (bottom) of the Duct configuration. (Gray) first iteration, (Black) second Iteration, (Dashed blue) $\hat{p}_k$ from direct eigenvalue problem Eqn. (8). (Dashed red) $\hat{p}_k^\dagger$ from adjoint eigenvalue problem Eqn. (9). Note that gray and black curves overlap the blue and red curves due to the good agreement, which verifies the proposed algorithm.

FIGURE 7. Thermoacoustic modes $\hat{p}/\max(\hat{p})$ (top) and $\hat{p}^\dagger/\max(\hat{p}^\dagger)$ (bottom) of the BRS configuration. (Gray) first iteration, (Black) second Iteration, (Dashed blue) $\hat{p}_k$ from direct eigenvalue problem Eqn. (8). (Dashed red) $\hat{p}_k^\dagger$ from adjoint eigenvalue problem Eqn. (9). Note that gray and black curves overlap the blue and red curves due to the good agreement, which verifies the proposed algorithm.
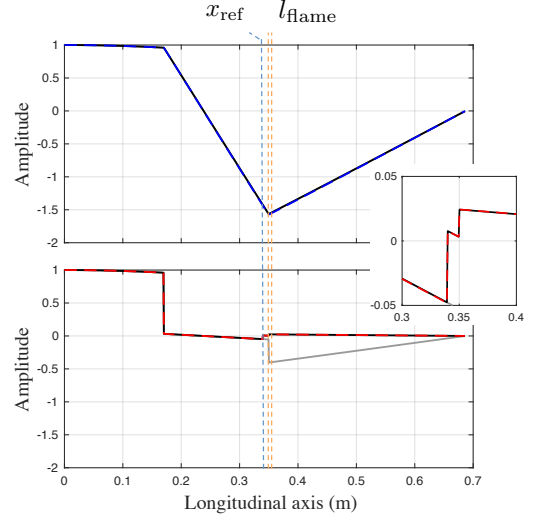
Such an adjoint sensitivity study can be carried out for any other system's parameter, such as time delay τ or acoustic reflection at

TABLE 3. Eigenfrequencies under consideration

Case	$\omega_{g_0} = 2\pi \cdot 1/(2\tau) + i \cdot 0$	ω_k (from Eqn. (9))
D1	$2\pi \cdot 416.667 + 0\,i$	$2\pi \cdot 416.667 - 0.00089\,i$
D2	$2\pi \cdot 312.5 + 0\,i$	$2\pi \cdot 312.485 - 0.004\,i$
B1	$2\pi \cdot 91.667 + 0\,i$	$2\pi \cdot 91.667 + 0\,i$
B2	$2\pi \cdot 68.75 + 0\,i$	$2\pi \cdot 68.75 + 0\,i$

the boundaries, at zero extra cost.

FIGURE 8. Locus of eigenfrequencies in the complex plane of the Duct configuration. Note that this figure is an extract of Fig. 3. The red lines indicate the slope (sensitivity $\partial \omega / \partial n|_{\omega_{g_0}}$) computed with the adjoint method.
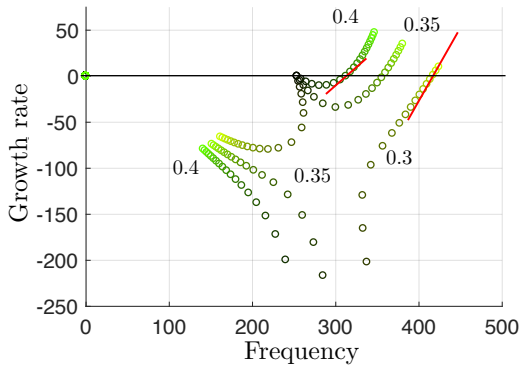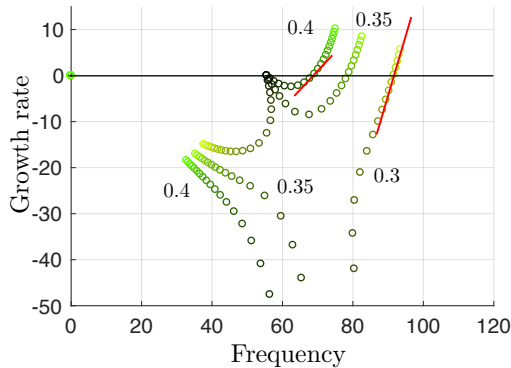

FIGURE 9. Locus of eigenfrequencies in the complex plane of the BRS configuration. Note that this figure is an extract of Fig. 4. The red lines indicate the slope (sensitivity $\partial \omega / \partial n|_{\omega_{g_0}}$) computed with the adjoint method.

Main parameters affecting the critical gain

By studying Eqn. (11), it is possible to understand which thermodynamics and geometrical parameters can make a combustor prone to thermoacoustic instabilities or, in other words, to identify under which conditions Eqn. (11) gives low values of n_{g_0}. Letting aside the influence of ω and τ, we realize that a combustor described by the terms $(\hat{p}_k^\dagger)^H \mathscr{A} \hat{p}_k$ and $(\hat{p}_k^\dagger)^H \mathscr{H} \hat{p}_k$ with low and large values, respectively, is prone to exhibit thermoacoustic instability for low values of the interaction index n.

Let us first analyze the term $(\hat{p}_k^\dagger)^H \mathscr{A} \hat{p}_k$ for the four cases investigated, whose values are shown in Tab. 4. When comparing D1 against B1 and D2 against B2, it is observed that low values of this term does not imply necessarily low values of n_{g_0} (last column of Tab. 4). Therefore, analyzing $(\hat{p}_k^\dagger)^H \mathscr{A} \hat{p}_k$ does not give clues about which parameters control the stability of the combustors investigated. Therefore, we analyze the term

$$\mathscr{T} = (\hat{p}_k^\dagger)^H \mathscr{H} \hat{p}_k = (\hat{p}_k^\dagger)^H I_{\mathrm{d}} \,\theta \bar{c}_{\mathrm{ref}}^2 S_{\mathrm{ref}}/(S_{\mathrm{f}}\, l_{\mathrm{f}}) \left. \frac{\partial \hat{p}_k}{\partial x} \right|_{\mathrm{ref}} \quad (17)$$

to evaluate under which conditions it exhibits large values. By looking at Eqn. (17) we realize that $\mathscr{T}$ is proportional to θ, $\bar{c}_{\mathrm{ref}}^2$, $S_{\mathrm{ref}}/S_{\mathrm{f}}$ and $1/l_{\mathrm{f}}$. The corresponding values for the Duct and BRS configurations are displayed in table 5. The parameters θ, $\bar{c}_{\mathrm{ref}}$ and l_{f} have similar values for both BRS and duct systems. In contrast, we observe that the area ratio $S_{\mathrm{ref}}/S_{\mathrm{f}}$ associated with the Duct configuration is approximately one order of magnitude larger than the one corresponding to the BRS combustor. This result implies that low values of $S_{\mathrm{ref}}/S_{\mathrm{f}}$ contribute to the stability conditioning of a combustor. Another factor of high impact on the value of $\mathscr{T}$ is the product $(\hat{p}_k^\dagger)^H I_{\mathrm{d}} \; \partial \hat{p}_k/\partial x|_{\mathrm{ref}}$. This parameter multiplies the value of $\hat{p}_k^\dagger$ at the flame region by the value of $\partial \hat{p}_k/\partial x$ at the reference position. Its value is given in table 4 for the four cases under study. The Duct configuration through cases D1 and D2 exhibits values of $(\hat{p}_k^\dagger)^H I_{\mathrm{d}} \; \partial \hat{p}_k/\partial x|_{\mathrm{ref}}$ which are almost two order of magnitudes larger than the counterparts B1 and B2 of the BRS combustor. In retrospect, it is possible to understand why the Duct combustor exhibits values of n_{g_0} which are significantly smaller than the ones corresponding to the BRS system and, therefore, is more prone to manifest thermoacoustic instabilities.

We conclude the study by highlighting the importance of the parameter $\mathscr{T}$, which in one term summarizes the contributions of all thermodynamic and geometrical parameters on the stability of a quasi-1D thermoacoustic system. We realize also that this parameter plays a crucial role in the description of $\partial \omega / \partial n|_{\omega_{g_0}}$ as evidenced in Eqn. (14). It is also important to remark that the present study can be extended to fully 3D combustors, where, as performed in the present work, the influence of flame location-distribution and combustor geometry on the stability of the sys-

9

2018 by ASME

tem are encapsulated in the operator $\mathscr{H}$ and both direct and adjoint eigenvectors.

TABLE 4.   Parameters of interest

Parameter	$(\hat{p}_k^\dagger)^H \mathscr{A} \, \hat{p}_k$	$(\hat{p}_k^\dagger)^H I_{\mathrm{d}} \left. \frac{\partial \hat{p}_k}{\partial x} \right\vert_{\mathrm{ref}}$	n_{g_0}
D1	2.4119e+05	-0.0187	0.723
B1	2.2442e+05	-0.0028	3.156
D2	-1.8196e+06	-0.0110	0.353
B2	-8.9071e+04	$-9.09\cdot10^{-4}$	1.718

TABLE 5.   Parameters influencing the term $\mathscr{T}$

Parameter	BRS	Duct
θ	5.5870	4.4608
l_{f}	0.0014	0.001
$\bar{c}_{\mathrm{ref}}^2$	117730	117810
$S_{\mathrm{ref}}/S_{\mathrm{f}}$	0.1303	1

CONCLUSIONS

The thermoacoustic modes at the region of marginal stability of two different quasi-1D combustors with full acoustically reflecting boundary conditions were investigated. Aside from the passive thermoacoustic modes, whose resonance frequency is strongly related to the geometry of the system, it was found that the eigenfrequency associated with the thermoacoustic modes at the neutral curve is entirely defined by the dynamics of the flame and, therefore, independent of the geometry of the combustor. These observations were obtained by analyzing the locus of the eigenfrequencies in the complex plane for parametric variations of n and τ, where also was recognized that the obtained plots for the two systems under study are alike. This finding is of relevance when characterizing the acoustic activity of an unstable combustor, where resonance frequencies may be related not only to (perturbed) passive thermoacoustic modes but also to ITA modes.

In the second part of the article, a method is proposed to evaluate at a very low computational cost the critical gain and corresponding sensitivity at the neutral curve. This method makes use of the direct and adjoint acoustic eigenvectors. The methodology here exposed may be used to quantify how prone a given combustor is to exhibit combustion instabilities independently of a particular flame response. For example, very high values of critical gain (for diferent values of τ) would imply a robustly stable combustor.

While carrying out the computations needed for the locus plot, it was found that assessing the eigenfrequency values for the quasi-vertical (ITA) trajectories (the ones whose growth rate decays to infinity for decreasing values of n) by solving the nonlinear eigenvalue problem is a challenging task. It was necessary to use very low values of the relaxation coefficient (around 0.05) when applying the fix point iteration method in order to assure convergence of the results. This may be one of the reasons why Helmholtz solvers have not been yet widely used for the study of ITA modes. With the method proposed in the second part of the paper it is possible not only to assess the values of the eigenfrequencies at the region of marginal stability, but also the corresponding direct and adjoint eigenvectors by solving a few times a linear system instead of a nonlinear eigenvalue problem.

REFERENCES

[1] Lieuwen, T., and Yang V., (Eds.), 2005. "Combustion instabilities in gas turbine engines: operational experience, fundamental mechanisms and modeling". *Prog. in Astronautics and Aeronautics AIAA, 210*.

[2] Candel, S., 2002. "Combustion dynamics and control: Progress and challenges". *Proc. Combust. Inst., 29*, pp. 1–28.

[3] Durox, D., Schuller, T., Noiray, N., and Candel, S., 2009. "Experimental analysis of nonlinear flame transfer functions for different flame geometries". *Proc. Combust. Inst., 32*, pp. 1391–1398.

[4] Kim, K., Lee, J., Quay, B., and Santavicca, D., 2010. "Spatially distributed flame transfer functions for predicting combustion dynamics in lean premixed gas turbine combustors". *Combust. Flame , 157*, pp. 1718–1730.

[5] Tay-Wo-Chong, L., Bomberg, S., Ulhaq, A., Komarek, T., and Polifke, W., 2012. "Comparative validation study on identification of premixed flame transfer function". *J. Eng. Gas Turb. and Power, 134*(2), pp. 021502–1–8.

[6] Silva, C. F., Emmert, T., Jaensch, S., and Polifke, W., 2015. "Numerical study on intrinsic thermoacoustic instability of a laminar premixed flame". *Combust. Flame , 162*, pp. 3370–3378.

[7] Keller, J. J., 1995. "Thermoacoustic Oscillations in Com-

bustion Chambers of Gas Turbines". *AIAA Journal, 33*(12), pp. 2280–2287.

[8] Nicoud, F., Benoit, L., and Sensiau, C., 2007. "Acoustic modes in combustors with complex impedances and multi-dimensional active flames". *AIAA Journal, 45*, pp. 426–441.

[9] Silva, C. F., Nicoud, F., Schuller, T., Durox, D., and Candel, S., 2013. "Combining a Helmholtz solver with the flame describing function to assess combustion instability in a premixed swirled combustor". *Combust. Flame , 160*(9), pp. 1743–1754.

[10] Emmert, T., Meindl, M., Jaensch, S., and Polifke, W., 2016. "Linear State Space Interconnect Modeling of Acoustic Systems". *Acta Acustica united with Acustica, 102*(5), pp. 824–833.

[11] Crocco, L., 1951. "Aspects of combustion instability in liquid propellant rocket motors. Part I". *J. American Rocket Society, 21*, pp. 163–178.

[12] Crocco, L., 1952. "Aspects of combustion instability in liquid propellant rocket motors. Part II". *J. American Rocket Society, 22*, pp. 77–16.

[13] Poinsot, T., and Veynante, D., 2012. *Theoretical and numerical combustion*. R. T. Edwards.

[14] Hoeijmakers, M., Kornilov, V., I. Lopez Arteaga a, d. P. d. G., and Nijmeijer, H., 2014. "Intrinsic instability of flame-acoustic coupling". *Combust. Flame , 161*(11), pp. 2860–2867.

[15] Emmert, T., Bomberg, S., and Polifke, W., 2015. "Intrinsic thermoacoustic instability of premixed flames". *Combust. Flame , 162*(1), pp. 75–85.

[16] Courtine, E., Selle, L., and Poinsot, T., 2015. "DNS of Intrinsic Thermoacoustic Modes in Laminar Premixed Flames". *Combustion and Flame, 162*(11), pp. 4331–4341.

[17] Silva, C. F., Merk, M., Komarek, T., and Polifke, W., 2017. "The Contribution of Intrinsic Thermoacoustic Feedback to Combustion Noise and Resonances of a Confined Turbulent Premixed Flame". *Combustion and Flame, 182*, pp. 269–278. bibtex: SilvaMerk17.

[18] Mukherjee, N., and Shrira, V., 2017. "Intrinsic Flame Instabilities in Combustors: Analytic Description of a 1-D Resonator Model". *Combustion and Flame, 185*, pp. 188–209. bibtex: MukheShrir17.

[19] Komarek, T., and Polifke, W., 2010. "Impact of swirl fluctuations on the flame response of a perfectly premixed swirl burner". *J. Eng. Gas Turbines Power, 132*(6), June, pp. 061503–1,7.

[20] Albayrak, A., Steinbacher, T., Komarek, T., and Polifke, W., 2017. "Convective Scaling of Intrinsic Thermo-Acoustic Eigenfrequencies of a Premixed Swirl Combustor". *J. Eng. Gas Turbines and Power*.

[21] Magri, L., and Juniper, M. P., 2013. "Sensitivity analysis of a time-delayed thermo-acoustic system via an adjoint-based

approach". *Journal of Fluid Mechanics, 719*, pp. 183–202.

[22] Magri, L., Bauerheim, M., and Juniper, M. P., 2016. "Stability analysis of thermo-acoustic nonlinear eigenproblems in annular combustors. Part I. Sensitivity". *Journal of Computational Physics, 325*, pp. 395 – 410.

[23] Magri, L., and Juniper, M. P., 2014. "Adjoint-based linear analysis in reduced-order thermo-acoustic models". *Int. J. Spray Combust. Dyn., 6*(3), pp. 225–246.

[24] Silva, C., Magri, L., Runte, T., and Polifke, W., 2017. "Uncertainty quantification of growth rates of thermoacoustic instability by an adjoint Helmholtz solver". *J. Eng. Gas Turbines and Power, 139*(1).

A Relation between $\hat{p}_k$, $\hat{p}_k^\dagger$ and $\tilde{p}_k$, $\tilde{p}_k^\dagger$

The Helmholtz Equation reads

$$\mathscr{A}\hat{p}_k + \omega_k^2\hat{p}_k - \mathscr{H}\mathscr{F}(\omega)\hat{p}_k = 0 \qquad (18)$$

where $\hat{p}_k$ and ω_k^2 are the k_{th} eigenvector and eigenfrequency of the active thermoacoustic system. Let us now assume that the active acoustic eigenvectors can be well represented by a linear combination of the passive acoustic eigenvectors as $\hat{p}_k = \sum_{k=1}^{N} \hat{p}_{k_p}\eta_{k_p}$, where N is the number of modes considered and η_{k_p} are weighting coefficients. Equation (18) reads now

$$\mathscr{A}\sum_{k=1}^{N}\hat{p}_{k_p}\eta_{k_p} + \omega_k^2\sum_{k=1}^{N}\hat{p}_{k_p}\eta_{k_p} - \mathscr{H}\mathscr{F}(\omega)\sum_{k=1}^{N}\hat{p}_{k_p}\eta_{k_p} = 0 \quad (19)$$

By recalling that the passive eigenvalue problem is defined by $\mathscr{A}\hat{p}_{k_p} = -\omega_{k_p}^2\hat{p}_{k_p}$, we rewrite Eqn. (19) as

$$-\sum_{k=1}^{N}\hat{p}_{k_p}\omega_{k_p}^2\eta_{k_p} + \omega_k^2\sum_{k=1}^{N}\hat{p}_{k_p}\eta_{k_p} - \mathscr{H}\mathscr{F}(\omega)\sum_{k=1}^{N}\hat{p}_{k_p}\eta_{k_p} = 0$$
$$(20)$$

By exploiting the biorthogonality between $\hat{p}_{k_p}$ and $\hat{p}_{k_p}^\dagger$, which means $(\hat{p}_{k_p}^\dagger)^H\hat{p}_{l_p} = \delta_{kl}$, we project Eqn. (20) on to the basis of the adjoint eigenvectors. Equation (20) becomes

$$\omega_k^2\eta_{k_p} - \omega_{k_p}^2\eta_{k_p} - \underbrace{(\hat{p}_{k_p}^\dagger)^H\mathscr{H}\mathscr{F}(\omega)\sum_{k=1}^{N}\hat{p}_{k_p}\eta_{k_p}}_{s_a} = 0 \qquad (21)$$

We consider now the last term s_a of Eqn. (21) to be a forcing term that acts exclusively in the region of the flame. Rearranging

Eqn. (21), we obtain

$$\eta_{k_p} = \frac{(\hat{p}_{k_p}^\dagger)^H s_a}{\omega_k^2 - \omega_{k_p}^2} \quad \text{and subsequently} \quad \hat{p}_k = \sum_{k=1}^{N} \hat{p}_{kp}\, \eta_{k_p}, \quad (22)$$

The vector s_a is the unknown. Therefore, we consider a vector s that acts as a uniform (with trivial value) forcing term in the region of the flame. In this study we set $s = I_d$. The solution of this problem is given by

$$\tilde{\eta}_{k_p} = \frac{(\hat{p}_{k_p}^\dagger)^H s}{\omega_k^2 - \omega_{k_p}^2} \quad \text{and subsequently} \quad \tilde{\hat{p}}_k = \sum_{k=1}^{N} \hat{p}_{kp}\, \tilde{\eta}_{k_p}, \quad (23)$$

or directly by solving the linear system

$$\mathscr{A}\, \tilde{\hat{p}}_k + \omega_k^2 \tilde{\hat{p}}_k = s \qquad (24)$$

Note that the vectors s_a and s are proportional. As a result, the active acoustic eigenvector $\hat{p}_k$ can be considered proportional to $\tilde{\hat{p}}_k$. This can be understood if comparing Eqn. (22) to Eqn. (23). By carrying out a similar analysis, we can find $\tilde{\hat{p}}^\dagger$ by solving

$$\mathscr{A}^H \tilde{\hat{p}}^\dagger + \omega_k^{*2} \tilde{\hat{p}}^\dagger = s, \qquad (25)$$

where $\tilde{\hat{p}}^\dagger$ is considered proportional to the adjoint eigenvector $\hat{p}^\dagger$. We need to find now a correct scaling. This is done by normalizing $\tilde{\hat{p}}$ and $\tilde{\hat{p}}^\dagger$ as

$$\hat{p}_k = \frac{\tilde{\hat{p}}_k}{\sqrt{(\tilde{\hat{p}}_k^\dagger)^H \tilde{\hat{p}}_l}} \quad \text{and} \quad \hat{p}_k^\dagger = \frac{\tilde{\hat{p}}_k^\dagger}{\sqrt{(\tilde{\hat{p}}_k^\dagger)^H \tilde{\hat{p}}_l}}, \qquad (26)$$

so that $(\hat{p}_k^\dagger)^H \hat{p}_k = 1$ is satisfied.